Generated using the official AMS LaTeX template v6.1

On the MJO Phase Speed Among Different Background Moisture and Zonal Wind Base States

Ahmed Shaaban and Paul Roundy

Department of Atmospheric and Environmental Sciences, University at Albany, State University of New York, Albany, New York, USA

Corresponding author: Ahmed Shaaban, alasheen@albany.edu

Current affiliation: Department of Atmospheric and Environmental Sciences, University at Albany, State University of New York, Albany, New York, USA.

ABSTRACT: The variability of the phase speed of the Madden Julian oscillation (MJO) is poorly understood. The authors assess how the phase speed of the convective signal of the MJO associates with the background states over Eastern Africa and the Indian Ocean. ~~Relaxation of the coupling between the convective MJO (intraseasonal moisture) and its circulation has been previously linked to faster propagation of MJO circulation signals east of the Dateline.~~ Relaxation of the coupling between tropical modes and their circulation has been previously linked to faster propagation; for example, MJO speeds up over Eastern Pacific where its convective signal decouples from the circulation. In contrast, our results show that fast MJO events happen to exist during periods of wetter background states (> 90 days) from East Africa across the Indian Ocean, whereas slow MJO is associated with dry background states. We found that fast MJO exhibits strong active and inactive phases with structure suggesting more hierarchical convection. Results indicate that the association of the phase speed of the MJO as seen in the integrated filtered moist static energy with the its tendency is stronger than the association of the phase speed as observed in the dry static energy with its tendency which is consistent with the acceleration of the MJO during wet background states. Also, our results indicate the MJO may be faster during periods of enhanced low-level moisture because these periods have anomalously weak upper tropospheric easterly background wind, which reduces the westward advection of the MJO by the background easterly wind, resulting in higher eastward phase speed of the MJO. The acceleration of the MJO by the background zonal wind overwhelms the deceleration associated with the moist wave dynamics.

SIGNIFICANCE STATEMENT: This study shows that the Madden Julian oscillation (MJO), which is the dominant subseasonal weather signal in the tropics, moves eastward more quickly across Eastern Africa and the Indian Ocean when the region is abnormally moist. The faster propagation does not appear to result from the higher moisture, but instead from encountering weaker than normal upper air winds from the east that tend to occur during moist periods.

1. Introduction

The Madden Julian oscillation (MJO; Zhang 2005) is the dominant intraseasonal mode in the tropics. Although there is no consensus on its dynamics or how to best trace its signal (Straub 2013), the MJO could be described as a cluster of convection coupled with large-scale atmospheric circulation moving eastward with an average speed of 5 m s^{-1} over the warm pool. Its associated large-scale circulation accelerates eastward over the Eastern Pacific, where coupling to convection is much weaker (Salby and Hendon 1994; Bantzer and Wallace 1996).

The unsettled dynamics of the MJO and the variety of indices used to trace it (e.g., Straub 2013) complicate studying the variability of MJO phase speeds. One of the earliest simple models of the MJO was a slow Kelvin wave (e.g. Chang and Lim 1988, and many others) as both MJO and Kelvin waves move eastward and couple with convection. This avenue retains some esteem, as it is supported by recent observations; for example, ~~structures similar to Kelvin waves emerge in the upper troposphere over the Indian Ocean from data filtered for the MJO.~~ the upper tropospheric circulation signal associated with the MJO over the Indian Ocean appears as a Kelvin ridge to the east of the convection and a Kelvin wave trough to the west (Roundy 2020). The Kelvin wave trough to the west cannot be forced by convection to its east, as that convection would drive a ridge. Nevertheless, the horizontal structure of the MJO, in general, includes substantial non-Kelvin features leading some to describe it as a Rossby-Kelvin wave couplet (e.g., Rui and Wang 1990) or quadrupole vortex (e.g., Monteiro et al. 2014) which has been considered in recent theorizing of the MJO (e.g., Skeleton model of the MJO Majda and Stechmann 2009). Such structures raise debate on the role of the forced Rossby wave component in modulating the phase speed of the MJO (Wang et al. 2018). ~~In contrast, the upper tropospheric circulation signal associated with the MJO over the Indian Ocean appears as a Kelvin ridge to the east of the convection and a Kelvin~~

~~wave trough to the west (Roundy 2020). The Kelvin wave trough to the west cannot be forced by convection to its east, as that convection would drive a ridge.~~

Aside from the gravity wave perspective of the MJO as simplified by Kelvin and tropical Rossby waves, the theory of the moisture mode (e.g., Sobel et al. 2014) arose as a different pathway to understand the propagation and evolution of the MJO. Under the gravity wave perspective, gravity is the restoring force for barotropic waves, and buoyancy (reduced gravity) is the restoring force for baroclinic flow ~~waves traveling in stratified flow~~. Under the moisture mode hypothesis, the evolution and the propagation of the MJO could be traced by moisture or moist static energy field. For instance, fluctuations of moist static energy in phase with precipitation, not only on the intraseasonal scale but also on the background and synoptic scales (Inoue and Back 2015). The convective initiation of the MJO is preceded by the advection of lower tropospheric background moisture by the easterly wind associated with the previous MJO event (Zhao et al. 2013; Li et al. 2015; Zhu and Hendon 2015). The research also suggests that the horizontal advection of background moisture by the MJO flow is essential for the northward propagation of the MJO during northern summer (Jiang et al. 2020). Moreover, the termination of MJO convection is preceded by negative anomalies of moisture over the equatorial Indian Ocean (Stachnik et al. 2015).

Analysis of the moist static energy budget has suggested several potential mechanisms that might explain the dynamics of MJO propagation. Benedict and Randall (2007) analyzed the structure of moisture associated with maximum rainfall and found that shallow convection precedes the maximum rainfall associated with the MJO, and dryness driven by horizontal advection follows the peak precipitation by few days, and in roughly 1 ~ 2 weeks succeeded by vertical advection of dry air. Maloney (2009) found that charging of MSE occurs during MJO easterlies and meridional advection of the MSE is the dominant contributor to change in the MSE via suppression of the synoptic eddies. In an aqua-planet model, Andersen and Kuang (2012) found that the tendency of moist static energy is in phase with horizontal advection of the background moisture by the MJO flow, suggesting that horizontal advection may contribute to the eastward propagation. The same results have been replicated by Hsu and Li (2012) using ECWMF Reanalysis ERA-40, and by Sobel et al. (2014) using data from the Dynamics of the MJO (DYNAMO) field program. Kim et al. (2014) found that MJO events that actively propagate over the western Pacific were associated with a poleward advection of the MSE by the synoptic eddies (including tropical Rossby waves), which eventually distribute the MSE over a wide meridional area. Moreover, Wang et al. (2017) compared the MSE structure in models associated with propagating versus non-propagating MJO signals. They found that the MSE is in quadrature with the MSE tendency in the models with propagating MJO, while the MSE is in phase with the MSE tendency in the models with non-propagating MJO. Their distinction between propagating and non-propagating MJO depends on inclusion of westward Fourier components, so it is possible that MJO-events deemed non-propagating emerge from the interference pattern generated by superposition between MJO and equatorial Rossby wave signals and thus still include propagating MJO signals.

Using aqua-planet simulations, Jiang et al. (2020) found that the simulated intraseasonal oscillation propagates westward if a prescribed uniform SST (which produces an off-equatorial peak in moisture) is used instead of SST gradients (which yield a moisture maximum at the equator). It is unclear the extent to which the mechanisms in subseasonal variability in these models conform to the mechanisms in observations, including the different factors in models and observations that determine the time mean balance between eastward and westward-moving intraseasonal modes. Indeed, the extent to which the upper tropospheric circulation signal associated with the MJO resembles Kelvin wave both east and west of the convection (Roundy 2020), eastward propagation may be assured without any of these mechanisms. Besides, low frequency of the occurrence of the MJO events in models might ultimately wash out their bulk signal in the power spectrum and regression analysis, and mislead our understanding of representation of the MJO in global models (Ling et al. 2017).

Aside from the exact nature of the MJO, MJO convective events evolve in a region from East Africa across Indian Ocean with known upper tropospheric easterlies. Roundy (2022) estimated the 200 hPa background zonal wind associated with the MJO at various phase speeds. He found that the slowest MJO events are most affected by the background upper easterlies, and that in resting atmosphere without steering wind, the phase speed of the MJO exceeds 10 m s^{-1}. Hence, Variability of the MJO phase speed could be explained in terms of the variability of the background zonal wind.

The proposed essential role of advection of background moisture by the MJO wind for the initiation and termination of MJO convection, the propagation versus the stalling of the MJO, and the eastward versus the westward propagation of proposed simple model disturbances suggest the idea that the background moisture or MSE could modulate MJO phase speed. Previous work on moisture mode theory has suggested relationships between the phase speed of the MJO and moisture gradients. Other works have suggested that increased convective activity, increased moisture, and increased precipitation rates are associated with slower MJO signals. Hence, we analyze the variability of the MJO phase speed with different states of the background moisture at different locations over the Indian Ocean and Eastern Africa. Although the moisture mode theory applies the gradient of the background moisture to predict the characteristics of the moist wave, this study does not, in essence, test a particular theory. Since this area has not been studied enough, this study analyzes the characteristics (speed and structure) of the MJO in different background setups. We think there is merit to analyzing raw variables (e.g., background moisture or wind) before analyzing more derived quantities (e.g., gradient of background moisture or wind).

Section 3 discusses the technique used to filter the data for the MJO band and the regression technique used to isolate the structure of the MJO at different background moisture levels. The variability of the MJO phase speed with background moisture is presented in section 4a. The vertical structure of the MJO associated with different phase speeds is discussed in section 4b. Analysis of the moisture budget at different background moisture conditions is explained in section 4c. Finally, in section 4d, we show the background zonal wind states associated with the fast and slow MJO. Results investigate to what extent moisture and the background flow are associated with varying phase speed of the MJO. A subsequent paper will discuss a similar analysis of the relationship between zonal and meridional gradients of moisture and MJO phase speed.

2. Data

Horizontal wind, vertical wind, temperature, specific humidity and geopotential height data were obtained from the ECMWF Interim Reanalysis (ERA-I, Dee et al. 2011) on 2.5°x2.5° grid and 32 vertical pressure levels, from 1980 to 2016, extending from 180°E to 180°W and from 20°S to 20°N at 00, 06, 12, and 18 UTC. Daily resolution was produced by averaging the 6-hourly dataset. The ERA-I moisture dataset incorporates SSM/I satellite data (Trenberth et al. 2011), making it suitable for analyzing the moisture field over the Indian Ocean.

The daily grided NOAA outgoing longwave radiation (OLR) dataset was obtained from 1979 to 2017 on a 2.5° × 2.5° grid (Liebmann and Smith 1996).

In order to budget the latent heat (moisture, see section 4c), we downloaded the following variables from the ERA-I dataset:

- Precipitation and evaporation (in meters) are accumulated forecasted variables, so their analysis time and accumulated period must be specified. To get the daily precipitation, we downloaded the data at 00 and 12 UTC with a 12-hour forecast accumulation, so are summed over 00 and 12 UTC accumulation data. To put the precipitation and evaporation (both in meters of water) in energy units (W m^{-2}), we multiplied the daily sum amount of precipitation or evaporation by $\frac{\rho \times L_v}{24 \times 60 \times 60}$, where ρ is the density of water (1000 kg m^{-3}) and L_v is the latent heat of evaporation (2.45 × 10^6 J kg^{-1}). Hence, the Evaporation of one meter of precipitation per day requires 28 × 10^3 W m^{-2}. Conversion of the units of precipitation and evaporation into energy units is necessary for consistency with the vertically averaged budget variables, as discussed in section 4c. Precipitation is a model-dependent variable in ERA-interim and ERA-5 since station precipitation inputs are not used. ERA-I is known for its wet biases over equatorial central Africa. Yet, it has a better precipitation representation than its predecessor data (ERA-40) and represents the interannual variability and annual cycles well.

- Sensible heat and latent heat, defined as positive for downward fluxes. To get their daily total values, we downloaded them at 00 and 12 UTC with a 12-hour forecast step, as we did with the precipitation and evaporation.

- Net radiation in the atmospheric column. To calculate it, we downloaded surface net solar flux, surface net thermal, top net solar radiation, and top net thermal radiation at 00 and 12 UTC with 12-hour accumulation, as we did before. Those parameters are positive for downward fluxes. The unit of the fluxes is J m^{-1} and to convert it into Watt m^{-2}, we divided by the time of the accumulation period 12 hours, 12 × 60 × 60 seconds. Other flux datasets could outperform ERA-I, but at the same time, using different data from the rest of the project raises more problems with the closure of the budget, making it rather difficult to understand the dynamics under investigation.

3. Methods

a. Spatial-temporal data filtering.

We used the discrete Fourier transformation (DFT) to extract the intraseasonal component of the ERA-I zonal wind, geopotential height, and specific humidity. This Fourier filtering technique uses a boxcar approach which can cause Gibbs ringing lobes, especially near the ends of the filtered dataset, so we only use data between 1980 and 2016. To distinguish the MJO from westward-moving signals (Wang and Rui 1990), we filter to retain only eastward-propagating components by selecting wavenumbers 1 - 10 and the Fourier harmonics for the 20 - 90 day range using two dimensional DFT following Kiladis et al. (2005); Straub (2013) and many others. The Broader wavenumber range is essential to account from the small scale convective activity associated with the MJO, including harmonics to its dominant wavenumber, and makes the results less sensitive to the domain size and the filter design (Straub 2013; Roundy and Schreck III 2009). Besides the intraseasonal components, we estimate the background states by lowpass filtering data for periods longer than 90 days, retaining the long-term mean and seasonal cycle as well as interannual and longer term variability.

Several indices have been used to trace MJO convective signal or large-scale circulation or both (Straub 2013). It is convenient to use an MJO index that traces the MJO convective signal when analyzing the relationship between the background moisture and convective-MJO. Following Zhao et al. (2013), we constructed an MJO index using only OLR data to analyze the convective initiation of the MJO. The covariance matrix of the 20 - 90 day filtered OLR anomalies confined between 40°E to 180°E and 30°S to 30°N was constructed by taking $X^T X$, where X is a array whose columns are the time series at each grid point. The principal component time series were found by projecting the filtered OLR anomalies onto the eigenvectors of this matrix. We used the first principle component (PC1) as a predictor in the regression models to analyze the structure of the MJO. All analysis is based on the northern winter MJO from November to April, when MJO activity peaks (Zhang and Dong 2004). Narrower merdional domain from 20°S to 20°N, used by other authors, yields the same EOF components as the larger domain (not shown), with correlation of -0.99 between the larger and smaller domains first PCs. The domain extends from 40°E to 180°E to account for the active and inactive phases of the MJO.

PC1 is used as base index for the regression and composite analysis. Lag regression against PC2 ultimately leads to similar conclusions at time lags. This is the case because the two EOFs and PCs are in quadrature in space and time, so they have a maximum lag correlation at 90-degree phase shifts, otherwise, they could not represent a propagating pattern from an EOF analysis. Both indices combined, at time lag zero, could describe any phase state of the MJO. We typically use a pair of indices in real time because they combine to tell us the present state, effectively at a zero-time lag. On the other hand, for composite or regression analysis as conducted in this paper, a time lag from one index alone can be used to represent the MJO signal generated from any combination of the two original PCs, based on the extent of the association between the two PCs at 90-degree shift. Regression analysis senses only the time scales associated with the PC1. Variables other than the OLR data may be associated with horizontal scales that extend outside the filtered wavenumbers when regressed against PC1. Those scales would appear in the regression maps and might result in different estimates of the speed of the MJO in the non-OLR filtered variables.

The real-time multivariate MJO index (Wheeler and Hendon 2004, RMM index) has been used to reproduce some results in section a.

b. The varying-coefficients regression technique.

Roundy (2017) developed a regression technique for providing regression coefficients that vary continuously across the seasonal cycle. Standard linear regression can be applied to find a single set of coefficients corresponding the predictors. When calculated based on data from different times of the year, linear regression yields different coefficients. This new algorithm predicts what the coefficients would be in particular ~~background~~ conditions such as particular days of year. The algorithm uses regression of the variance of the predictor against the leading harmonic of the seasonal cycle, and regression of the covariance between the predictor and predictand against the same leading harmonic of the seasonal cycle. The ratio of covariance and variance coefficients on a given day of the year ~~to estimate~~ is the regression slope coefficient most likely to apply on that day. A revision of the technique is used here to find regression coefficients that fluctuate with any slowly varying signal instead of the seasonal cycle. The varying regression technique (Roundy 2017) is superior to the partial regression technique (Yule 1907) used to find the correlation between two variables while excluding their linear fluctuation with an other (third) variable that might impact the correlation value, in the sense that the algorithm reveals the impact of a third variable on the regression coefficient.

In this study, we use the varying regression coefficients technique to analyze the structure and the speed of the MJO in different background moisture states, which may be of essence to the initiation and the propagation of the MJO (see sec. 1). A time lag regression model of the evolving MJO structure is achieved by regressing fields of data against a predictor MJO index x. Let y represent a particular dependent variable at some grid point and time lag. Our objective is to find the regression slope coefficient relating x and y as the relationship varies with background moisture. The technique is as follows: (1) regress the time series of the squared values of MJO index, x^2, on the slowly varying background moisture. The regressed values represent the regressed variance of the predictor; (2) regress the product of the MJO index with the times series of the dynamical field that we are interested to analyze against the background moisture. Similarly as in step 1, the output represents the regressed covariance. This dynamical field serves as the regressed variable; (3) substituting the value of the background moisture in (2) and (1) to find the predicted covariance and the predicted variance, and then their ratio is the regression coefficient associated with the prescribed value of the background moisture.

In theory, we can use the traditional linear regression technique for a subset of the data that occurs within a range of background values we are interested in. Yet, the varying regression technique introduced by Roundy (2017) leverages the whole data set since the actual selection of the background is performed after calculating the slopes. Utilizing the whole dataset in the varying regression technique makes the resultant signal clearer and more statistically robust than the traditional regression technique that looks at general background states in isolation.

c. Statistical test.

We used the students t-test to test the statistical significance of the traditional regressions and composites. Yet implementing a parametric statistical test is challenging when considering the varying-coefficients regression that includes multiple regressions (Roundy 2017). Hence, we used a bootstrap test following Roundy (2017) to study the statistical significance of the varying-coefficients regression. To implement the test, the regression coefficients are calculated 10,000 times based on random samples from the original data, with samples taken with replacement (see ch. 5 Wilks 2011, for details on the bootstrap technique). Those coefficients constitute the population distribution with similar autocorrelation characteristics. To test the significance of the regression coefficient against, for example, the 90% level, we check if the calculated regression coefficient is confined between the population confidence interval, which is between 500 and 9,500 quantiles.

4. Results

a. MJO phase speed among varying background moisture states.

To get a better idea of the structure of the MJO that is associated with the PC1 index (defined in Section 3), we present lead-lag regression Hovmöller diagram of the filtered zonal wind at 850 and 200 hPa (Figs. 1a and b), and specific humidity at 850 hPa (Fig. 1c). At 850 hPa, over the Indian Ocean, westerly anomalies are located west of the negative OLR anomalies, with easterly anomalies to the east. The reverse occurs at 200 hPa, consistent with the traditional vertical structure of the MJO that maps roughly onto the first barocinic mode or ~~higher baroclinic mode~~ the superposition of the first few baroclinic modes (Rui and Wang 1990, and others) that ultimately resembles an overturning circulation. The quadrature relationship between the wind and convection resembles MJO model I of Zhang and Anderson (2003, Fig. 1). At day zero, specific humidity at 850 hPa peaks over the Indian Ocean, while negative values cover central and eastern Pacific Ocean (Fig. 1c). Those structures (Figs. 1a-c) are similar to the MJO structure between phases 2 and 3 of the RMM index (Wheeler and Hendon 2004), where the impact of the active phase of the MJO convection lies over the Central Indian Ocean. Over the Indian Ocean, the specific humidity is in quadrature with the 850 hPa zonal wind (Figs. 1a and c) and in phase with the MJO convection center. This intraseasonal moisture anomaly might be important for maintaining the MJO convective activity, yet the initiation and the propagation of the MJO itself have been hypothesized to be supported by the advection of background moisture, rather than intraseasonal moisture, by the lower tropospheric easterly zonal wind associated with the previous MJO event (Zhao et al. 2013; Straub 2013).

The phase speed of the MJO as represented by the regressed zonal wind anomaly at 850 hPa is roughly 5.6 m s^{-1} (see reference line on Fig. 1a). The reference lines that mark the phase speed of the contours, subjectively fit the peak contours between -10 and 9 days in all Hovmollor except in section c, where we choose to fit field between -15 to 5 days as some fields decays rapidly. For some figures, we draw another reference line for the phase speed that fits maximum contours only over the Indian Ocean between 60°E and 110°E. For clarity, we refer to the phase speed of the reference line that fit the maximum contours between -10 and 9 day as the phase speed and phase speed represented by the reference line over the Indian Ocean as the Indian Ocean (IO) phase speed. The phase speed of zonal wind at 200 hPa (Fig. 1b) is faster than the 850 hPa zonal wind. The regression technique captures those signals that correlate with the index rather than the signal propagating at a particular phase speed. This indicates that the maximum power of the 200 hPa filtered zonal wind at a particular wavenumber does not align with the maximum power of the 850 hPa filtered zonal wind at the same wavenumber. The vertical tilted or stacked baroclinic structure of the MJO circulation changes over its lifetime, which must imply that associated circulation anomalies move at moderately different speeds as the vertical structure evolves to lead to the different vertical alignments between them. The abrupt acceleration of the MJO signal, represented by the upper and lower layer zonal wind and specific humidity (Figs. 1a-c), near the dateline has been understood as a result of the separation between the circulation and convection that were coupled over the Indian Ocean (Salby and Hendon 1994, and many others), but also incursion of the extratropical Rossby wave response to west Pacific convection back into the tropics via the westerly wind duct of the Western Hemisphere (e.g., Sakaeda and Roundy 2015). The IO phase speed of the 200 hPa zonal wind signal matches the IO phase speed of the 850 hPa moisture signal, yet the 200 hPa zonal wind over the Indian Ocean happen to be centered near day -10, whereas the 850 hPa moisture signal over the Indian Ocean lies around day 0. This indicate the upper wind signal leads the lower moisture signal over the IO. Upper level easterlies have been found to be favorable for the development of MJO (Roundy 2014)

To study the variability of the MJO phase speed with the background moisture, we reproduce the previous lagged regression Hovmöller diagrams, but at specific values of background moisture using the varying regression coefficient discussed in Section 3. In order to implement varying coefficient regression, we construct background moisture indices. Figure 2 shows box-plots of

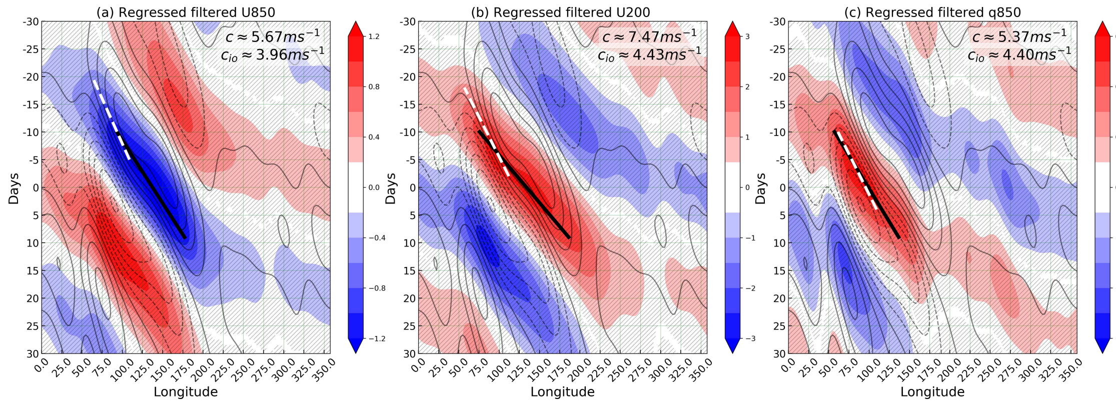

FIG. 1. Shaded contours are lagged regression of 20 - 90 days eastward filtered: (a) zonal wind at 850 hPa, shaded at an interval of 0.2 m s^{-1}, (b) zonal wind at 200 hPa, shaded at an interval of 0.5 m s^{-1}, and (c) specific humidity at 850 hPa, shaded at an interval of 0.05 g kg^{-1}. Contours are lagged regression of the 20 - 90 days eastward filtered OLR, contoured at an interval of 2 W m^{-2} from -12 W m^{-2}. All those variables were regressed against PC1 (see text for more information about the PC1). Hatched shaded areas are statistically significantly different from zero above the 90% level based on resampling 10,000 samples utilizing a bootstrap statistical test. The solid black reference lines approximate the phase speed of the contour lines peak between -10 and 9 days. The white dashed reference lines approximate the phase speed over the Indian Ocean between 60°E and 110°E. The phase speeds of the black reference line c and white reference line (over the Indian Ocean) c_{io} are listed respectively in the first and second rows in the upper right corner.

the background moisture over different regions proximate to the Indian Ocean. For the most part, the minimum, median, and maximum values of the background moisture increase from Eastern Africa to the Maritime continent while the total variance decreases eastward. This paper focuses on the MJO phase speed association with the background moisture over Eastern Africa proximate to the Indian Ocean ~~and the Indian Ocean.~~ We also analyze the variability of the MJO phase speed with background moisture over the western Indian Ocean, Eastern Indian Ocean, and the Maritime Continent regions as half of MJO convective events were reported to initiate over the Eastern Indian Ocean and Western Pacific (Matthews 2008; Straub 2013).

Figure 3 presents varying coefficient lag-regressions of the filtered zonal wind at 850 hPa when the background moisture over Eastern Africa is 7 g kg^{-1}, 9 g kg^{-1}, and 11 g kg^{-1}. Those values are close to the minimum, median, and maximum values of the background moisture (see Fig. 2), thus reflecting the phase speed of the MJO across the range of background moisture. The

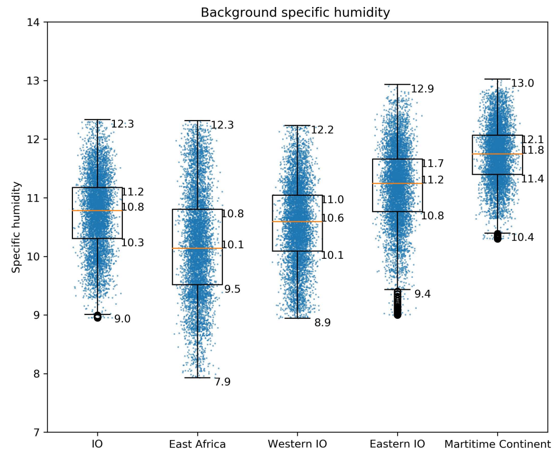

FIG. 2. Box-plots of the background (> 90 days) specific humidity over different locations, superimposed on scatter plots of the same variable that is spread horizontally using a random function to get an idea on the density of the background specific humidity at each value. The background specific humidity is averaged over the Indian Ocean basin (10°S - 10°N, 50°E - 90°E), East Africa (10°S - 10°N, 35°E - 55°E), Western Indian Ocean (10°S - 10°N, 55°E - 72.5°E), Eastern Indian Ocean (10°S - 10°N, 72.5°E - 90°E), and Maritime-continent (10°S - 10°N, 90°E - 107.5°E). The lower, middle and upper sides of the box-plot represent the first (Q1), second (median), and third (Q3) quarterlies, where the lower and upper fences represent the minimum and maximum values, and circles represent outliers. The outliers are values smaller than Q1-1.5*IQR or larger than Q3+1.5*IQR, where IQR is inter-quartile range=Q3-Q1.

phase speeds of the MJO, as represented by the filtered 850 hPa zonal wind, when the 850 hPa background moisture is 7, 9, and 11 g kg^{-1} are 4.3, 5, and 6 m s^{-1} (Fig. 3 a and c), suggesting that the phase speed of the MJO increases with the background moisture content at 850 hPa. The phase speed of the MJO using traditional linear regression (Fig. 1a), which is 5.6 m s^{-1}, lies between the upper and lower limit of the MJO phase speed found at 7 and 11 g kg^{-1} (Fig. 3a and c), indicating that the traditional regression expresses the weighted mean phase speed across the population of background moisture states. We reproduced Fig. 3 using background moisture over the Western Indian Ocean, Eastern Indian Ocean, and Maritime Continent, and found that the phase speed of the MJO also increases with the background moisture (not shown), consistent with the results using background moisture over Eastern Africa. The IO phase speed of the 850 hPa zonal wind signal increases when the background moisture increases from 9 to 11 g kg^{-1}, but decreases with further increases of the background moisture.

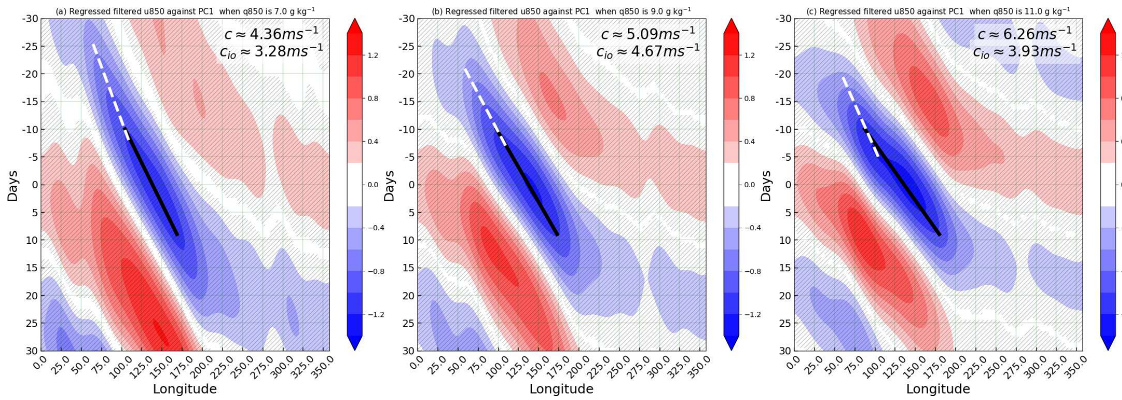

FIG. 3. Lagged regression of 20 - 90 days eastward filtered zonal wind at 850 hPa on PC1 when the background moisture over Eastern Africa is (a) 7 g kg^{-1}, (b) 9 g kg^{-1}, (c) 11 g kg^{-1}. Shading is in an interval of 0.2 m s^{-1}. Hatching indicates that the field is statistically significant from zero above the 90% level using a bootstrap statistical test.

Figure 4 presents the lagged zonal wind over 200 hPa associated with the background moisture over Eastern Africa. The inclusion of the wind data is important because the upper tropospheric wind might influence the MJO phase speed by advection. Strong upper tropospheric westerly anomalies over the equatorial Indian Ocean tend to occur with lower tropospheric easterly anomalies, which may increase the low-level moisture over the western Indian Ocean. The speed of the zonal wind at 200 hPa increases with the background moisture but at a slower rate than that of the zonal wind at 850 hPa. We produced the same figure using background moisture over the Western Indian Ocean, Eastern Indian Ocean, and Maritime Continent. We found that the increase of the phase speed with background moisture is largest when using background moisture over the Maritime Continent. Besides the observed increases in the phase speed of the filtered zonal wind with the background moisture, the amplitude of the filtered zonal wind intensifies, reflecting a stronger MJO signal in the variable (Fig. 4). The previous analyses were reproduced again using RMM index, and the increases of the phase speed of the dynamical fields associated with the MJO at different background moisture were observed. Contrary to the slight increases of the phase speed of the 200 hPa signal centered around day 0 (black reference line), the IO phase speed of the 200 hPa zonal wind signal increased by 43% when the background moisture raised from 7 to 9 g kg^{-1}, and amplified by 53% when the background moisture jumped from 9 to 11 kg^{-1}.

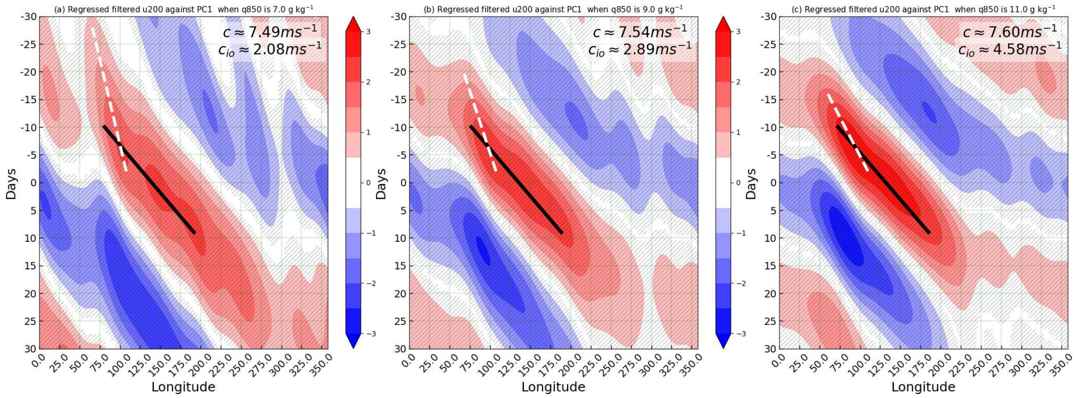

FIG. 4. The same Lagged regression in Fig. 3, except for the zonal wind at 200 hPa instead of zonal wind at 850 hPa.

To verify the results produced by the method of varying regression slope coefficients, we present Hovmöller diagrams that show composites of the 850 hPa filtered zonal wind at low and high 850 hPa background moisture as shown in Fig. 5. We composite around the days when time in PC1 exceeds one standard deviation simultaneous with background moisture values in its lowest quartile (Q1), including the outliers. We repeat the process for background moisture values in their highest quartile (Q2), Figure 5b. Our choice of selecting days associated with 1STD of PC1 and Q1 or Q2 is arbitrary but is the most common in the literature. A drawback of the composite analysis compared to the varying regression method is that we cannot find a clear structure representing the signal at a specific value of the background moisture because a composite requires a population of events over which to average. Figure 5 shows that the phase speeds of the filtered 850 hPa zonal wind at low and high moisture are 4.8 and 6.6 m s^{-1} consistent with the regression results.

b. The vertical structure of the MJO associated with different background moisture states.

Figure 6 presents the zonal-vertical structure of the zonal wind associated with PC1 when the background moisture is 7 g kg^{-1} and 12 g kg^{-1}, following the method of varying regression slope coefficients. The vertical structure of the zonal wind is stacked, where a positive anomaly field lies above a negative anomaly field or vice versa. The stacked structure is usually observed over the Indian Ocean, in contrast to the tilted structure, where tilted positive or negative signed anomalies extend across the vertical column, which is usually observed over the Maritime continent and the

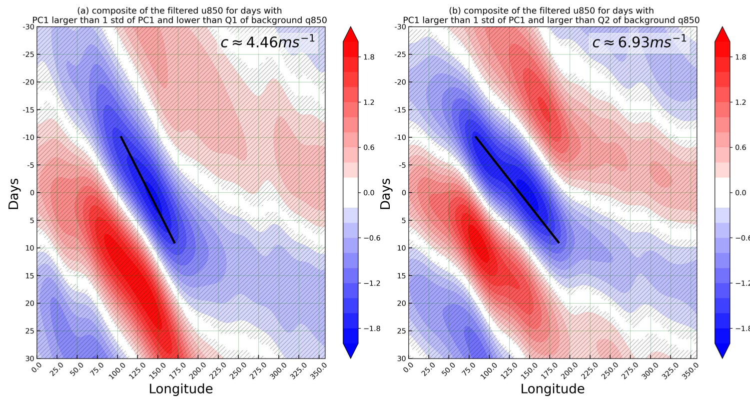

FIG. 5. Composites of the filtered zonal wind at 850 hPa for days with (a) PC1 larger than 1STD of PC1 and lower than Q1 of the 850 hPa background moisture, (b) PC1 larger than 1STD of PC1 and larger than Q2 of the 850 hPa background moisture. Shading is in an interval of 0.2 m s^{-1}. Hatching indicates that the underlying shading is statistically significantly different from zero at the 90% level using t-test analysis.

Pacific Ocean (Sperber 2003; Kiladis et al. 2005). At first glance, the two signed stacked structure of the zonal wind (Fig. 6) is consistent with the first baroclinic mode. Yet, the intensification of the zonal wind with height suggests that either barotropic mode or more baroclinic modes would be needed to account for either the intensified zonal wind above 500 hPa or the lessening of the zonal wind below 500 hPa structure (Rui and Wang 1990). On the other hand, the Kelvin wave part of the MJO could be understood as radiative wave, instead of a superposition between the baroclinic modes. Hence, the vertical structure of the MJO could be described in terms of radiative waves to the extent that Kelvin wave dynamics explain its structure (Roundy 2020). At 7 g kg^{-1} (Fig. 6a), the westward tilt of the zonal wind in the troposphere and the eastward tilt in the stratosphere suggest structure similar to the radiative structure of the Kelvin wave, with upward-energy transfer in the stratosphere and downward-energy in the troposphere (Shaaban and Roundy 2021). The vertical structure of the filtered zonal wind when the background moisture is 7 g kg^{-1} (Fig. 6a) is less stacked than that at 12 g kg^{-1} (Fig. 6b). Moreover, the upper level westerlies at 12 g kg^{-1} (Fig. 6b) are stronger than at 7 g kg^{-1} (Fig. 6a) over Eastern Africa and also over Maritime Continent (not shown), expressing stronger upper air outflow that might result from intensification of the convection.

Figure 7 shows regressed eastward 20 - 90 day filtered specific humidity associated with the 7 g kg^{-1} (Fig. 7a) and 12 g kg^{-1} (Fig. 7b) background moisture over Eastern Africa. The

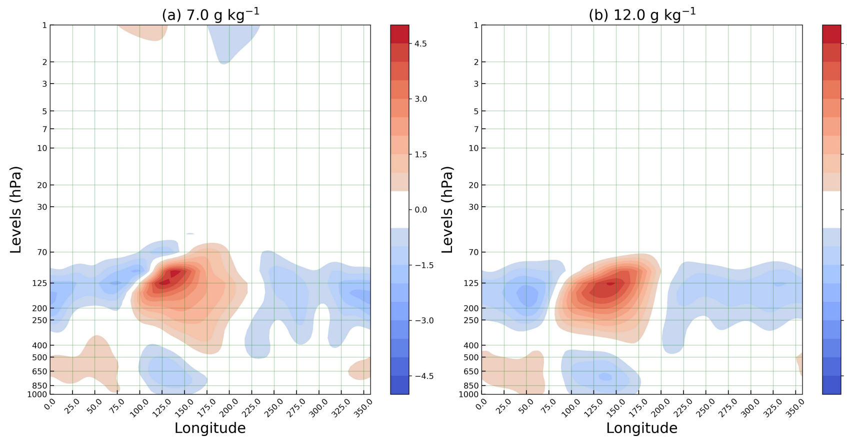

FIG. 6. Longitude-level maps of regressed eastward 20 - 90 days filtered zonal wind against PC1 when the 850 hPa background moisture is (a) 7 g kg^{-1}, (b) 12 g kg^{-1}. Shading is contoured every 0.4 m s^{-1}. Hatched contours are statistically significant different from zero above the 90% level using the bootstrap test.

maximum amplitude of the regressed intraseasonal filtered specific humidity (Fig. 7a) is less than the background specific humidity 7 g kg^{-1}; the same applied to Fig. 7b. The filtered specific humidity field shows a moist column over the Indian from surface to 300 hPa, consistent with the active convective phase of the MJO, and dry column over Western Pacific, consistent with the suppressed phase (Fig. 7). The intraseasonal specific humidity field associated with a high background moisture (12 g kg^{-1}) resembles wavenumber two, while it resembles wavenumber two or three at low background moisture (7 g kg^{-1}). The active phase over the Indian Ocean at 12 g kg^{-1} is wetter than that at 7 g kg^{-1}, also the suppressed phase over Western Pacific at 12 g kg^{-1} is drier than that at 7 g kg^{-1}. The active phase at 12 g kg^{-1} in the lower layer shows an eastward bulging structure that might be associated with shallow convection that precedes the MJO deep convection signal (Benedict and Randall 2007, and others), but since linear regression implies symmetry across opposite signs in the predictor, this result also applies to the dry phase at the same location.

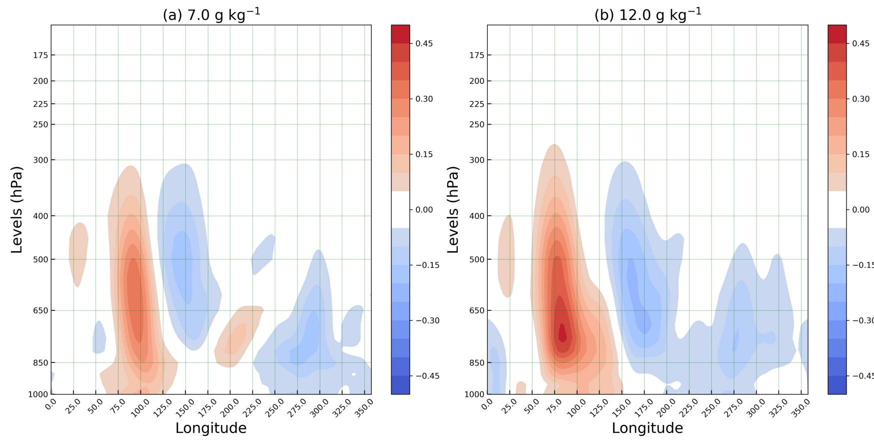

FIG. 7. Longitude-level maps of regressed eastward 20 - 90 days filtered specific humidity against PC1 when the 850 hPa background moisture over Eastern Africa is (a) 7 g kg^{-1}, (b) 12 g kg^{-1}. Shading is contoured every 0.4 m s^{-1}. Hatched contours are statistically significant from zero above the 90% level using bootstrap statistical test.

c. The relationship between the phase speed of the MJO and the intensity of the tendency of the moisture, dry, static energy, moist static energy.

Several authors have classified the MJO events produced by community global climate models (GCMs) into either propagating or non-propagating patterns based on the phase difference between the scalar field (e.g., moisture) used to represent MJO and the time tendency of that field. From a kinematics perspective, a scalar field is considered non-propagating (stationary) if it is in-phase with its tendency; for example, a low-pressure system tends to move to the region of the negative pressure tendency. On the other hand, the low-pressure system stalls if it is in phase with the pressure tendency field since the center of the low collocates with the region with the smallest negative pressure tendency (see section 2.1.4, Bluestein 1992). A quadrature phasing could be associated with either an eastward or westward propagation of the field under study. Although phasing status between the field and its tendency could be used to differentiate between the stationary and propagating MJOs, ~~tendency~~ phasing alone cannot determine phase speed because , for example, simple sinusoidal wave in quadrature with its tendency could have a continuum of phase speed, also, amplitude of the wave can vary, and amplitude also depends on tendency.

Alternatively, the speed of a trough or ridge pattern has been theorized, from a kinematic perspective, to be associated with the intensity of the tendency of the field under consideration , rather than the phasing between the field and tendency of the field, and the Laplacian of the field (see Petterssen formula for the speed of the scalar field patterns, section 2.1.4, Bluestein 1992). ~~This could be an alternative avenue to relate the phase speed with the field variable under study by using the amplitude of the field and its tendency rather than the phasing between them~~. One caveat of this approach is that the intensity of the tendency could vary with the field's amplitude at the same phase speed. We calculate the tendency of the moisture, dry static energy, and moist static energy fields, and if the amplitude approaches zero, the result blows up. Then, we investigate whether the acceleration of the MJO phase speed, as observed from the Hovmoller diagram of the moisture, is associated with the intensification of the tendency of the moisture field. We repeat the same analysis with dry and moist static energy.

The vertical average of the latent heat (an expression of the specific humidity in energy units, J kg^{-1}) $< Lq >'$ expressed in J m^{-2} and its tendency $< \partial_t Lq >'$ in W m^{-2} are computed, where q is the specific humidity in kg (of dry air) kg^{-1} (of water vapor) and $L = 2.5 \times 10^6$ m^2 s^{-2} is the latent energy of condensation or evaporation at 0°C. The bracket refers to the mass-weighted vertical average, defined as $\langle () \rangle = \frac{1}{g} \int () dp$ in kg m^{-2}. We choose layers between 1000 and 150 hPa (25 vertical levels) to calculate the vertical average of the moisture and the tendency, as this could be used later to calculate the moisture and energy budget terms. The prime refers to the intraseasonal scale defined in section 3. The vertical average of the dry static energy $\langle S \rangle'$ and its tendency $\langle \partial_t S \rangle'$ are also calculated. The dry static energy S is defined as $S = c_p T + gz$, where $c_p = 1004$ K m^2 s^{-2} is the heat capacity at constant pressure and $g = 9.8$ m s^{-2} is gravity. We used the moist static energy besides the moisture and dry static energy. The moist static energy $h = Lq + S$ is the sum of the latent heat and dry static energy.

Figure 8 depicts the vertical average of the MJO moisture (contoured) and MJO moisture tendency (shaded) when the background moisture is low (8 g kg^{-1}) and relatively high (12 g kg^{-1}) over Eastern Africa. At day 0, for both slow and fast MJO, the positive tendency is to the east of the moisture field, indicating eastward propagation. At low background moisture (Fig. 8a), the regressed fields of the vertical average of the intraseasonal moisture tendency and moisture are slower and longer-lived than that at high background moisture (Fig. 8b), as expected. The intraseasonal moisture field retains the same phase shift with its tendency irrespective of the background moisture. This result has been confirmed by investigating the phase shift at other background moisture values between the 8 and 12 g kg^{-1}. The magnitude of the tendency increases with the background speed, which is is consistent with Hu and Li (2022) who found that the tendency intensifies with fast MJO signals. The moisture tendency, at high background moisture (Fig. 8b), is prone to field discontinuity or reduction in the magnitude when passing over the Maritime Continent, which is not the case during the low background moisture. The discontinuity of the MJO depicted at (Fig. 8b) might represents a short hiatus over the Maritime Continent.

As depicted in Fig. 9, the magnitude of the DSE tendency is much smaller than moisture tendency; that is why it is sometimes neglected when compared to moisture tendency in the moist static energy analysis (Inoue 2016). The DSE tendency is small in the tropics since the temperature tendency is small and potential energy is smaller than sensible heat. The small of the horizontal gradient and the tendency of temperature leads to *weak temperature gradient* approximation (Sobel et al. 2001). In agreement with the analysis of the moisture field, the DSE and its tendency preserve the same phase shift irrespective of the background condition, as depicted in Fig. 9. The intensity of the DSE tendency among the slow and fast MJO events are comparable (Fig. 9), in contrast with the MSE (Fig. 8). Analysis of the phase shift between MSE and its tendency (not shown) also agrees with the previous results of the DSE and moisture.

Using the moisture budget equation, we investigate the terms (e.g., advection, forcing) that contribute to the charging or discharging of the intraseasonal moisture (i.e., increases or decreases of the tendency of q) at moist and dry background conditions, which could give us more insight on the characteristics of the tendency of the intraseasonal moisture at different phase speeds. Charging or discharging of moisture depends on the horizontal and vertical advection (first and second terms on the RHS of the equation), evaporation (third term on the RHS), and precipitation (last term on the RHS), as shown below.

$$\left\langle \frac{\partial Lq}{\partial t} \right\rangle' = -\langle V.\nabla(L\overline{q})\rangle' - \left\langle \omega \frac{\partial (Lq)}{\partial p} \right\rangle' + LE' - LP' \quad (1)$$

V and ω are the horizontal and vertical velocities. E and P are the evaporation and precipitation amounts. All terms are in W m^{-2}, which could be easily verified after noting that the mass-weighted vertical average has a unit of kg m^{-2}.

The horizontal advection of the moisture field, depicted in Fig. 10, is in phase with the moisture tendency; in other words, the horizontal advection charges the intraseasonal moisture field through

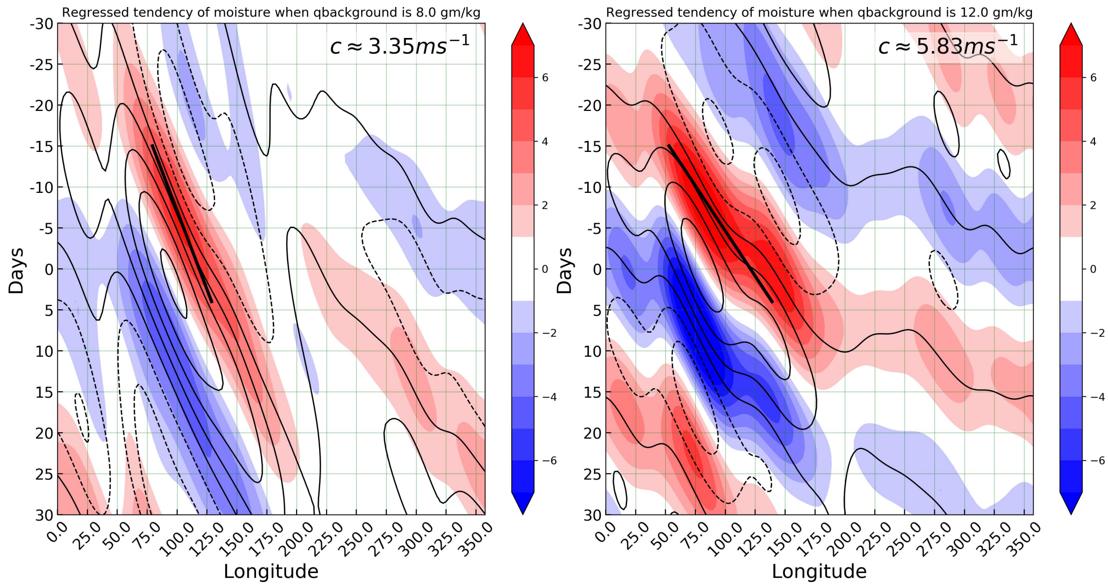

FIG. 8. Longitude-lag of regressed tendency of latent heat (shaded) and latent heat anomalies (contoured) averaged between -10° and 10° regressed against background specific humidity index over East Africa at 850 hPa at (a) 8 and (b) 12 gm kg^{-1}. Shading is contoured every 0.1 g kg^{-1}.

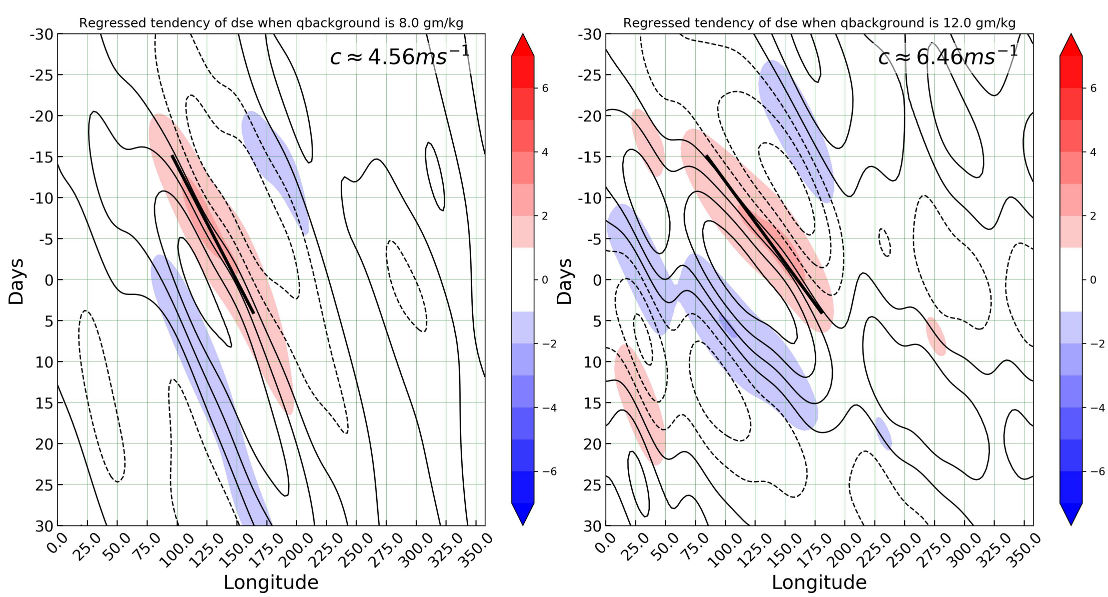

FIG. 9. Longitude-lag of regressed tendency of intraseasonal DSE (shaded) and intraseasonal DSE (contoured) averaged between -10° and 10° regressed against background specific humidity index over East Africa at 850 hPa at (a) 8 and (b) 12 gm kg^{-1}. Shading is contoured every 0.1 g kg^{-1}.

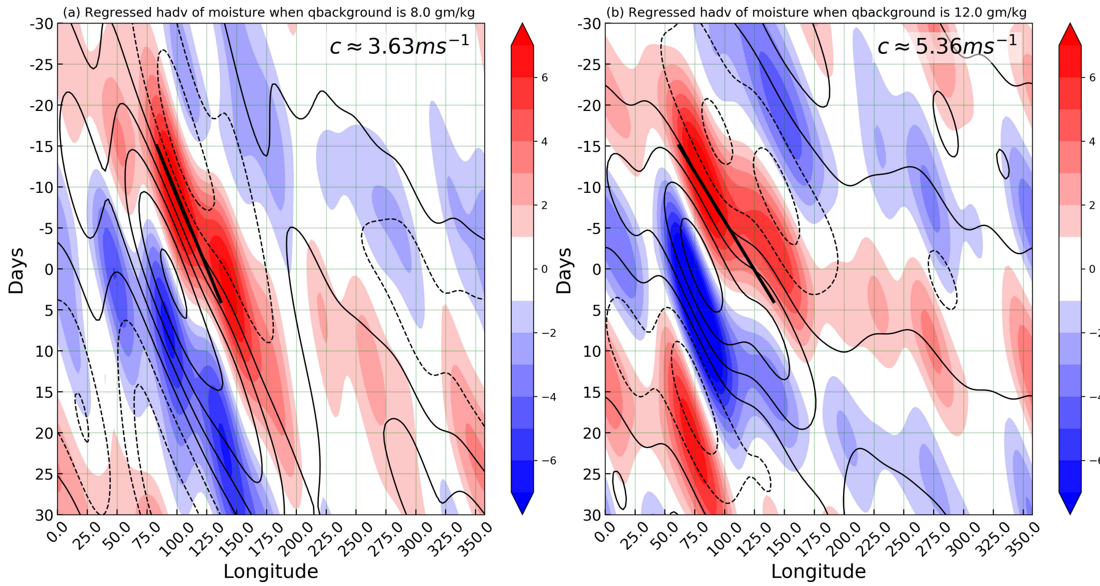

FIG. 10. Longitude-lag of regressed horizontal advection of intraseasonal moisture (shaded) and intraseasonal moisture (contoured) averaged between -10° and 10° regressed against background specific humidity index over East Africa at 850 hPa at (a) 8 and (b) 12 gm kg^{-1}. Shading is contoured every 0.1 g kg^{-1}.

the whole atmosphere. The readers may check that by either comparing the phasing between the tendency field with the advection field, which is in-phase, or by investigating the quadrature relationship between the moisture field and the advection as in Fig. 10. The phase speed of the horizontal advection of moisture increases with the background moisture (Fig. 10), which agrees with the behavior of the tendency field of the moisture. The phase speed of the advection of both moisture and DSE increases with the background moisture, which is in agreement with the tendency field. A clear discontinuity in the magnitude of the MJO horizontal (Fig. 10) and vertical advection (Fig. 11) fields presents over the Maritime Continent, during low and high background moisture states, which may indicate that MJOs crossing the Maritime Continent may have different dynamics from those over the Indian Ocean.

The horizontal advection of the intraseasonal DSE (not shown) is as small as the tendency field. In contrast to the moisture, the phase shift between the horizontal advection of the DSE field and its tendency is not even throughout the whole Hovmollar diagram, making it difficult to understand the overall role of the advection in charging or discharging the DSE field.

Figures 11 and 12 depict the vertical average of the vertical advection of the moisture and the vertical average of the forcing. Vertical advection and forcing dominate the moisture budget

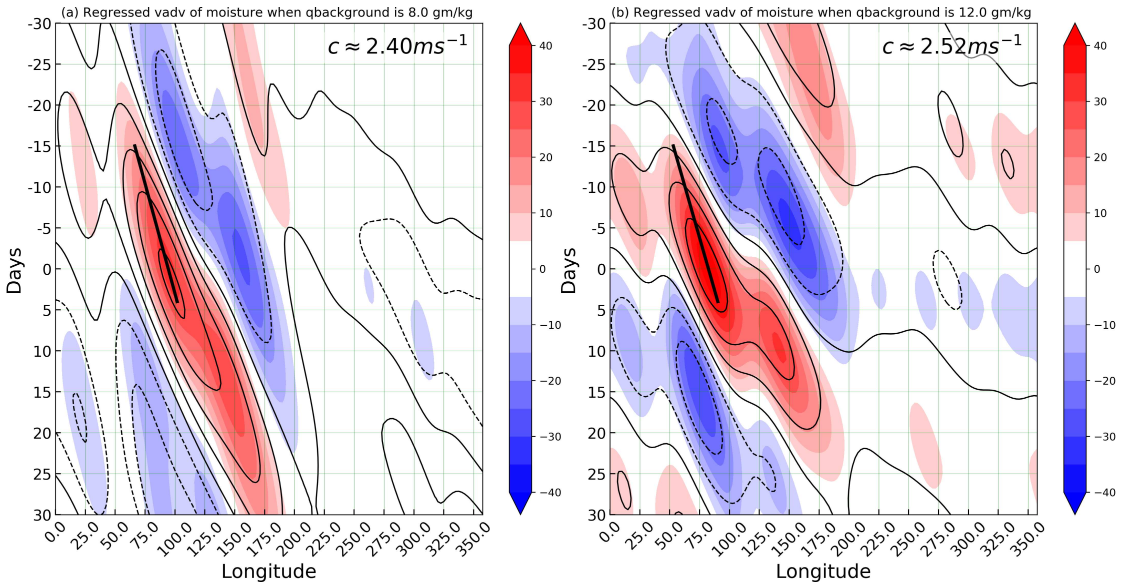

FIG. 11. Longitude-lag of regressed vertical advection of intraseasonal moisture (shaded) and intraseasonal moisture (contoured) averaged between -10° and 10° regressed against background specific humidity index over East Africa at 850 hPa at (a) 8 and (b) 12 gm kg^{-1}. Shading is contoured every 0.1 g kg^{-1}.

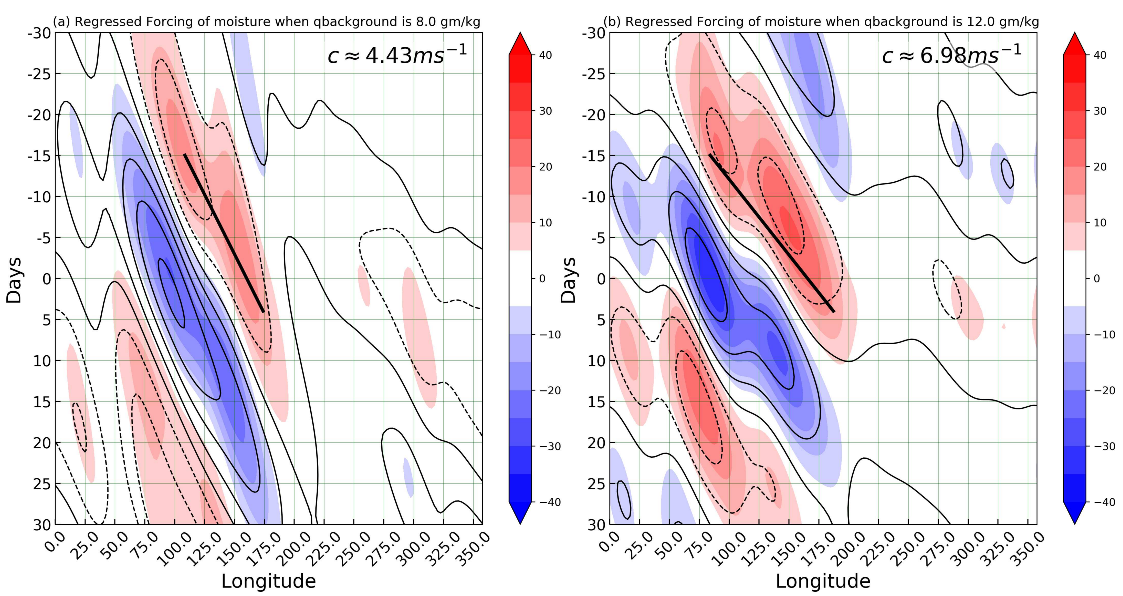

FIG. 12. Longitude-lag of regressed forcing (shaded) of intraseasonal moisture and intraseasonal moisture (contoured) averaged between -10° and 10° regressed against background specific humidity index over East Africa at 850 hPa at (a) 8 and (b) 12 gm kg^{-1}. Shading is contoured every 0.1 g kg^{-1}.

equation. The in-phase relationship between the vertical advection of the MJO moisture field and the MJO moisture field, depicted in Fig. 11, indicates that the vertical advection of moisture destabilizes moisture (i.e., increases moisture amplitude by vertically advecting moist air) instead of charging it (increasing moisture tendency). On the other hand, the forcing is out of-phase with the MJO moisture field, as depicted in Fig. 12, suggesting that the forcing stabilizes the moisture (decreases moisture amplitude by the excessive precipitation) instead of discharging it (i.e., decreasing moisture tendency). The vertical average of the vertical advection of the DSE charges the DSE, yet the forcing term discharges the DSE (not shown). The vertical advection and forcing cancel each other, though they have the largest amplitude in the DSE budget equation, as in the moisture budget. The structure of the MSE vertical advection (sum of DSE and moisture vertical advection) or MSE forcing (sum of the DSE and moisture forcing) differs from their counterpart in DSE and moisture. For example, while the vertical advection of DSE charges DSE, vertical advection of the moisture destabilizes the atmosphere, and the vertical advection of the MSE stabilizes the atmosphere, consistent with Inoue and Back (2015). The phase speed of the vertical integral of the vertical advection and forcing fields (Fig. 11 and 12) increases with background moisture. The field at dry background conditions is more continuous than that at 12 g kg^{-1}, which shows a rapid discontinuity at the Maritime Continent.

d. Advection by the Background Zonal Wind as an Alternative Explanation of Phase Speed Association with Humidity

To find a pathway that might connect the background moisture and the variability of the phase speed of the MJO over the Indian Ocean, we present the relationship between the background moisture over Eastern Africa and the upper level background zonal wind, which could alter the phase speed of the MJO by advection. Figure 13 shows the regressed slope (contours) background zonal wind against the background-specific humidity over Eastern Africa. The regressed slope background zonal wind shows weak lower-level easterlies and upper-level westerlies over the Indian ocean. This pattern agrees with the upper-level circulation during El Niño and positive Indian Ocean dipole, reflecting the weakening of the Walker circulation during Fall and spring associated with wet years over the western Indian Ocean and Eastern Africa (Shaaban and Roundy

2017). Nevertheless, the appearance of background upper-level westerlies over the Indian ocean is not common. To understand how such upper-level background zonal westerlies could appear in the regression slope term, we present the estimated background zonal wind (shaded, Figure 13), which is the sum of the intercept and the regressed slope coefficients values. The estimated background zonal wind depicts upper-level easterlies, consistent with the observed climatological background wind. The estimated background wind is easterlies since the intercept (not shown) depicts strong easterlies, which is way larger in magnitude than the regression slope coefficients.

Composite analysis could also be used to understand the previous association between the background moisture and zonal wind. Figure 14 depicts composites for the background zonal wind when 850 hPa background specific humidity is larger than its first quartile (Q1, hereafter wet events) as in (Fig.14a), and smaller than its second quartile (Q2, hereafter dry events) as in (Fig. 14b). Wet conditions over East Africa (Fig. 14a) are associated with weaker upper easterlies when compared with those associated with dry events (Fig. 14b). Weaker background easterlies during wet events over East Africa are a proxy for the build-up of upper-level background westerlies over the Indian Ocean associated with the convection near East Africa, which could be shown by subtracting background zonal wind of wet events from those of dry events (Fig. 14c).

Figure 13 was reproduced again but using background moisture over the western Indian Ocean, Eastern Indian Ocean, and Maritime Continent (not shown). We anticipated that the circulation pattern associated with the background moisture over the Maritime Continent would resemble a pattern opposite to that shown in Fig. 13, yet, surprisingly, we got circulations that also match El Niño and positive Indian Ocean dipole. This result suggests that the anomalous subsidence over the Maritime Continent raises the background moisture in the lower levels.

5. Discussion and conclusion

Although the region of the strongest rainfall variance of the MJO collocates with the region of maximum tropical precipitation and moisture, the relationship between the background moisture and propagation characteristics of the MJO has not been thoroughly investigated. This study uses a modulation regression technique to address the association of the MJO phase speed with low-level background moisture over Eastern Africa and the Indian Ocean. The lagged regressions of the

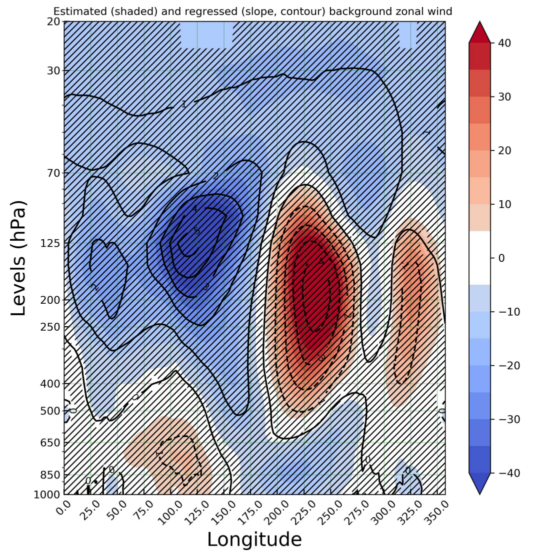

FIG. 13. Longitude-level of background (shaded) and background anomaly (contoured) of the zonal wind averaged between -10° and 10° regressed against background specific humidity index over East Africa at 850 hPa. Shading is contoured every 0.1 g kg^{-1}.

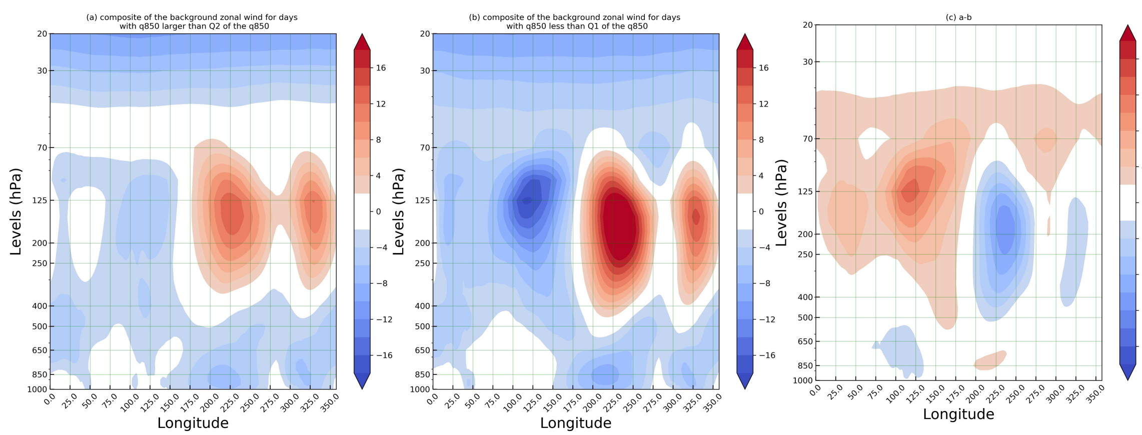

FIG. 14. Longitude-level composites of background zonal wind averaged between -10° and 10° (a) wet, (b) dry, (c) wet - dry at 850 hPa over East Africa.

MJO, as represented by the upper and lower level zonal wind and moisture, show an increase of the MJO phase speed with increases of the low-level background moisture over Eastern Africa and the Indian Ocean (Fig. 3 and 4). There remains substantial debate about mechanisms that might influence the propagation and propagation speed of the MJO. Some authors have suggested that convection likely reduces the phase speeds of tropical modes. For example, shallower convection has been theorized to be associated with higher baroclinic modes that decrease the phase speed of the tropical mode. Also, a reduction in the effective static stability felt by waves in the convective environment could decelerate the wave speed (Zhang 2005; Kiladis et al. 2009). Our results suggest that, westward advection ~~of the upper tropospheric circulation signal~~ of the MJO by the upper tropospheric easterly background wind would slow the MJO, and abnormally strong tropical easterlies would cause abnormally slow propagation (Roundy 2022). Figure 13 shows that when lower tropospheric moisture is high over the tropical Indian Ocean, upper tropospheric background wind tends to be less easterly than average, which would yield faster eastward movement by this argument. Our results do not necessarily suggest that convection does not slow the MJO, but if it does, that outcome must be overwhelmed by other mechanisms acting in the opposite direction.

The intraseasonal moisture anomaly associated with fast MJOs resembles wavenumber one (Fig. 7a), while slower MJOs project onto higher wavenumbers (Fig. 7b). The moist phases of the fast MJO events include a bulging structure to the east, which is absent in the slow MJO. The bulging structure might be associated with a progressive pattern of shallow and congestus convection, which is theorized to moisten the atmosphere before the initiation of the deep convection (Benedict and Randall 2007). Hence, the relative absence of the shallow convection might reflect rather weaker and slower MJOs. In comparison with the composite vertical structure of the MJO, the bulging structure of the fast MJO suggests that baroclinic modes beyond the first baroclinic mode would be required to account for the bulging structure, consistent with Haertel et al. (2008), who suggested the baroclinic structure of the MJO could be represented mainly using the first two baroclinic modes. Yet, at the same time, adding more higher baroclinic modes as in the normal mode theory or adding more plane waves as in the radiative wave structure (Shaaban and Roundy 2021), would suggest a slower propagation of the MJO. Yet, the observed fast MJO indicates that the effect of the background wind must overcome the deceleration associated with the dynamics of the moist waves. Under the moisture mode umbrella, the strong active and inactive phase of the fast MJO during moist background state could be attributed to the intensified moisture tendency associated with the strong advection of the background moisture by the MJO flow.

The background moisture fluctuates with the fluctuation of the Walker circulation as in Fig 13. Weakening of the Walker circulation is associted with wet conditions over Eastern Africa. On the other hand, reversal of the Walker circulation is associated with reseveral in SST total field or anomalies. The SST is a key variable in parameterizing the lower moisture field. This might indicate that the association between bacground zonal wind and moisture are due to impact of the SST variability on background wind and moisture.

Sobel et al. (2014) found a moisture mode moving eastward under an equatorward moisture gradient and a weak horizontal temperature gradient. This moisture mode has been suggested as a foundation for MJO dynamics (e.g. Adames and Kim 2016; Chen and Wang 2019). Regressions set with high background moisture show higher amplitude intraseasonal moisture anomalies than regressions set with lower background moisture (Fig. 7), consistent with predictions of a moisture mode theory. We found that the acceleration of the MJO as observed in the moisture field is associated with intensification of the tendency of the moisture (Fig. 8), nevertheless intensification of the tendency could be associated with intensification of the amplitude of the signal at the same phase speed. On the other hand, the accelerated DSE field is not associated with clear intensification of the DSE tendency (Fig. 9). It is yet unclear whether the phase speed signal we observe in association with background moisture is consistent with leading moisture mode theories, which are focused on horizontal gradients of moisture more than the total background moisture. A subsequent paper will apply the above techniques to assess the associations of MJO phase speed with zonal and meridional moisture gradient configurations.

Aside from the moisture mode perspective of the MJO, Roundy (2020) found that the upper structure of the MJO resembles Kelvin ridge to the east and Kelvin trough to the west. Moreover, Roundy (2022) found that the phase speed are subject to advection by upper zonal flow. The background upper-level zonal wind, associated with high background moisture over Eastern Africa is less easterly than the seasonal average background wind when the lower tropospheric of the region is also anomalously moist, which would result in less westward advection, thereby yielding higher than average eastward phase speed, which is consistent with Roundy (2022). The magnitude of upper-level background zonal wind anomaly is comparable to the average phase speed of the MJO, strongly suggesting a role for the advection of the MJO by the background upper tropospheric flow. That is, the MJO may be faster in these moist environments because moist environments tend to be associated with upper tropospheric westerly wind anomaly, which would result in faster eastward propagation. After subtracting out the effect of advection by the upper tropospheric background wind, Roundy (2022) showed that the slowest MJO events are those near the center of its spectral peak, where average intensity of OLR anomalies is strongest. Yet the slowing effects of moist processes are evidently substantially weaker than these advection effects, especially for the slowest events that experience the greatest westward advection.

Advection by the background wind would impact the movement of MJO circulation signals at every pressure level. However, variability in background wind is a factor of 10 larger in the upper troposphere than the lower troposphere, so the advection of the MJO-associated ~~lower~~ upper tropospheric circulation in the upper troposphere must yield a far greater impact on the variability of the phase speed of MJO wind anomalies assessed at the same level. The effect of 1 m s^{-1} wind amplitude in the lower troposphere on MJO phase speed must be of the same order, while 5-10 m s^{-1} variations in the upper troposphere must be that much larger. What we do not demonstrate clearly is how the upper tropospheric wind signals lead to changes in the phase speed of the convection. One possible mechanism for future analysis is that the advancing upper tropospheric divergence signal associated with the MJO reduces total subsidence, thereby reducing convective inhibition, thereby increasing convection, which then drives the lower tropospheric circulation in line with the upper tropospheric wind (Powell and Houze Jr. 2015).

We found that the phase speed of the 850 hPa zonal wind and moisture signals increases gradually with the background moisture wind, which might be consistent with the moisture mode. The IO phase speed of the 200 hPa zonal wind (identified by the white reference line)shows association with the background moisture stronger than the 200 hPa zonal wind signal (black reference line). This is because weakening or strengthening of the IO Walker circulation cooccur with weakening or strengthening of the Pacific ocean Walker arm. The 200 hPa zonal wind signal signal has a wider zonal extension and happens to be influenced by the opposite circulation of Walker in the Indian Ocean and the Pacific. So while strong upper easterlies over the Indian Ocean advects MJO westward, strong upper westerlies over the Pacific Ocean advects the MJO eastward.

This study demonstrates that the role of the background zonal wind is not confined to the initiation of the MJO in the lower troposphere but it confirms that the upper tropospheric zonal wind modulates MJO phase speed by advection whether the MJO is goverened by moist wave dynamics or moisture mode. This study supports other studies that emphasize the role of the background state of the model in correctly simulating MJO events (e.g. Ling et al. 2017). Although background moisture and upper background zonal wind are related, they have separate role in developing comprehensive moist-wave theory of MJO. Under the umbrella of the moist-wave dynamics, background moisture may strengthen the convective MJO by advecting moist air, hence decelerating the MJO, while the weakening of the upper background zonal wind associated with the strengthened background moisture accelerates the MJO. On the other hand, under the perspective of the moisture mode, a stronger tendency of the intraseasonal moisture field observed during the periods of high moist background might accelerate MJO, acting to further increase the MJO speed accelerated by the background zonal wind. That is, a dispersion equation at resting atmosphere consistent with observations should explain part of the variability of the MJO phase speed via simple dynamics of the moisture mode or moist waves. Then, by incorporating the role of the advection by the upper zonal wind, which may overwhelm the intrinsic phase speed of the MJO at resting atmosphere, a comprehensive diagnostic of the variability of the phase speed of the MJO is achived. This is similar to the overwhelming role of the background wind in modulating the phase speed of the midlatitude Rossby wave.

~~More analysis is needed to estimate the evidently smaller role of subseasonal moist processes in modulating the phase speed of the MJO. Could a bulb of moisture be sustained by tropospheric level of support of moist static energy irrespective of the effect of the upper-level zonal wind? Alternatively, if a moist coupled upper tropospheric Kelvin wave is a good model of the MJO, the results presented here would suggest that the MJO might move faster across the Indian Ocean during moist periods because of advection by the anomalous westerly background wind that tends to occur in the basin at the same time.~~

Acknowledgments. We are grateful for comments and suggestions by three anonymous reviewers. This work was funded by the National Science Foundation grant numbers AGS1560627, AGS1757342, and AGS2103624 to Dr.Paul Roundy. We are grateful for NOAA for providing the OLR dataset, for ECWMF for providing the ERA-Interim dataset. This manuscript is based on chapter three of the first author's dissertation.

Data availability statement. Work done in this manuscript is based on ERA interim data produced at European Centre for Medium-Range Weather Forecasts and available to download at `https://climatedataguide.ucar.edu/climate-data/era-interim`. Outgoing longwave radiation is available at NOAA physical science division `https://psl.noaa.gov/data/gridded/data.olrcdr.interp.html`

References

Adames, A. F., and D. Kim, 2016: The MJO as a Dispersive, Convectively Coupled Moisture Wave: Theory and Observations. *Journal of the Atmospheric Sciences*, **73 (3)**, 913–941, https://doi.org/10.1175/JAS-D-15-0170.1, URL https://doi.org/10.1175/JAS-D-15-0170.1, https://journals.ametsoc.org/jas/article-pdf/73/3/913/4814955/jas-d-15-0170_1.pdf.

Andersen, J. A., and Z. Kuang, 2012: Moist Static Energy Budget of MJO-like Disturbances in the Atmosphere of a Zonally Symmetric Aquaplanet. *Journal of Climate*, **25 (8)**, 2782–2804, https://doi.org/10.1175/JCLI-D-11-00168.1, URL https://doi.org/10.1175/JCLI-D-11-00168.1, https://journals.ametsoc.org/jcli/article-pdf/25/8/2782/4006988/jcli-d-11-00168_1.pdf.

Bantzer, C. H., and J. M. Wallace, 1996: Intraseasonal Variability in Tropical Mean Temperature and Precipitation and Their Relation to the Tropical 40–50 Day Oscillation. *Journal of the Atmospheric Sciences*, **53 (21)**, 3032–3045, https://doi.org/10.1175/1520-0469(1996)053⟨3032:IVITMT⟩2.0.CO;2, URL https://doi.org/10.1175/1520-0469(1996)053⟨3032:IVITMT⟩2.0.CO;2, https://journals.ametsoc.org/jas/article-pdf/53/21/3032/3428136/1520-0469(1996)053_3032_ivitmt_2_0_co_2.pdf.

Benedict, J. J., and D. A. Randall, 2007: Observed Characteristics of the MJO Relative to Maximum Rainfall. *Journal of the Atmospheric Sciences*, **64 (7)**, 2332–2354, https://doi.org/

10.1175/JAS3968.1, URL https://doi.org/10.1175/JAS3968.1, https://journals.ametsoc.org/jas/article-pdf/64/7/2332/3619787/jas3968_1.pdf.

Bluestein, H., 1992: *Synoptic-dynamic Meteorology in Midlatitudes*. No. v. 1, Synoptic-dynamic Meteorology in Midlatitudes, Oxford University Press, URL https://books.google.com.eg/books?id=hrV1wgEACAAJ.

Chang, C.-P., and H. Lim, 1988: Kelvin Wave-CISK: A Possible Mechanism for the 30–50 Day Oscillations. *Journal of the Atmospheric Sciences*, **45 (11)**, 1709–1720, https://doi.org/10.1175/1520-0469(1988)045⟨1709:KWCAPM⟩2.0.CO;2, URL https://doi.org/10.1175/1520-0469(1988)045⟨1709:KWCAPM⟩2.0.CO;2, https://journals.ametsoc.org/jas/article-pdf/45/11/1709/3424173/1520-0469(1988)045_1709_kwcapm_2_0_co_2.pdf.

Chen, G., and B. Wang, 2019: Dynamic moisture mode versus moisture mode in MJO dynamics: importance of the wave feedback and boundary layer convergence feedback. *Climate Dynamics*, **52 (9-10)**, 5127–5143, https://doi.org/10.1007/s00382-018-4433-7.

Dee, D. P., and Coauthors, 2011: The era-interim reanalysis: configuration and performance of the data assimilation system. *Quarterly Journal of the Royal Meteorological Society*, **137 (656)**, 553–597, https://doi.org/10.1002/qj.828, URL https://rmets.onlinelibrary.wiley.com/doi/abs/10.1002/qj.828, https://rmets.onlinelibrary.wiley.com/doi/pdf/10.1002/qj.828.

Haertel, P. T., G. N. Kiladis, A. Denno, and T. M. Rickenbach, 2008: Vertical-mode decompositions of 2-day waves and the madden–julian oscillation. *Journal of the Atmospheric Sciences*, **65 (3)**, 813–833, https://doi.org/10.1175/2007JAS2314.1, URL https://doi.org/10.1175/2007JAS2314.1, https://doi.org/10.1175/2007JAS2314.1.

Hsu, P.-c., and T. Li, 2012: Role of the boundary layer moisture asymmetry in causing the eastward propagation of the madden–julian oscillation. *Journal of Climate*, **25 (14)**, 4914–4931, https://doi.org/10.1175/JCLI-D-11-00310.1, URL https://doi.org/10.1175/JCLI-D-11-00310.1.

Hu, F., and T. Li, 2022: Effect of vertical overturning circulation scale and moist static energy tendency on mjo phase speed. *Atmospheric and Oceanic Science Letters*, **15 (1)**, 100 150, https://doi.org/https://doi.org/10.1016/j.aosl.2022.100150, URL https://www.

sciencedirect.com/science/article/pii/S1674283422000034, center for Climate System Prediction Research (CCSP).

Inoue, K., 2016: Moist static energy budget analysis over the tropical ocean. Ph.D. thesis, University of Wisconsin, Madison.

Inoue, K., and L. Back, 2015: Column-Integrated Moist Static Energy Budget Analysis on Various Time Scales during TOGA COARE. *Journal of the Atmospheric Sciences*, **72 (5)**, 1856–1871, https://doi.org/10.1175/JAS-D-14-0249.1, URL https://doi.org/10.1175/JAS-D-14-0249.1, https://journals.ametsoc.org/jas/article-pdf/72/5/1856/3664878/jas-d-14-0249_1.pdf.

Jiang, X., E. Maloney, and H. Su, 2020: Large-scale controls of propagation of the madden-julian oscillation. *NPJ Climate and Atmospheric Science*, **3 (1)**.

Kiladis, G. N., K. H. Straub, and P. T. Haertel, 2005: Zonal and vertical structure of the madden–julian oscillation. *Journal of the Atmospheric Sciences*, **62 (8)**, 2790–2809, https://doi.org/10.1175/JAS3520.1, URL https://doi.org/10.1175/JAS3520.1, https://doi.org/10.1175/JAS3520.1.

Kiladis, G. N., M. C. Wheeler, P. T. Haertel, K. H. Straub, and P. E. Roundy, 2009: Convectively coupled equatorial waves. *Reviews of Geophysics*, **47 (2)**, https://doi.org/10.1029/2008RG000266, URL https://agupubs.onlinelibrary.wiley.com/doi/abs/10.1029/2008RG000266, https://agupubs.onlinelibrary.wiley.com/doi/pdf/10.1029/2008RG000266.

Kim, D., J.-S. Kug, and A. H. Sobel, 2014: Propagating versus nonpropagating madden–julian oscillation events. *Journal of Climate*, **27 (1)**, 111 – 125, https://doi.org/https://doi.org/10.1175/JCLI-D-13-00084.1, URL https://journals.ametsoc.org/view/journals/clim/27/1/jcli-d-13-00084.1.xml.

Li, T., C. Zhao, P.-c. Hsu, and T. Nasuno, 2015: Mjo initiation processes over the tropical indian ocean during dynamo/cindy2011. *Journal of Climate*, **28 (6)**, 2121–2135, https://doi.org/10.1175/JCLI-D-14-00328.1, URL https://doi.org/10.1175/JCLI-D-14-00328.1.

Liebmann, B., and C. A. Smith, 1996: Description of a complete (interpolated) outgoing longwave radiation dataset. *Bulletin of the American Meteorological Society*, **77 (6)**, 1275–1277, URL http://www.jstor.org/stable/26233278.

Ling, J., C. Zhang, S. Wang, and C. Li, 2017: A new interpretation of the ability of global models to simulate the mjo. *Geophysical Research Letters*, **44 (11)**, 5798–5806, https://doi.org/https://doi.org/10.1002/2017GL073891, URL https://agupubs.onlinelibrary.wiley.com/doi/abs/10.1002/2017GL073891, https://agupubs.onlinelibrary.wiley.com/doi/pdf/10.1002/2017GL073891.

Majda, A. J., and S. N. Stechmann, 2009: The skeleton of tropical intraseasonal oscillations. *Proceedings of the National Academy of Sciences*, **106 (21)**, 8417–8422, https://doi.org/10.1073/pnas.0903367106, URL http://www.pnas.org/content/106/21/8417, http://www.pnas.org/content/106/21/8417.full.pdf.

Maloney, E. D., 2009: The moist static energy budget of a composite tropical intraseasonal oscillation in a climate model. *Journal of Climate*, **22 (3)**, 711 – 729, https://doi.org/https://doi.org/10.1175/2008JCLI2542.1, URL https://journals.ametsoc.org/view/journals/clim/22/3/2008jcli2542.1.xml.

Matthews, A. J., 2008: Primary and successive events in the madden–julian oscillation. *Quarterly Journal of the Royal Meteorological Society*, **134 (631)**, 439–453, https://doi.org/10.1002/qj.224, URL https://rmets.onlinelibrary.wiley.com/doi/abs/10.1002/qj.224, https://rmets.onlinelibrary.wiley.com/doi/pdf/10.1002/qj.224.

Monteiro, J. M., Á. F. Adames, J. M. Wallace, and J. S. Sukhatme, 2014: Interpreting the upper level structure of the Madden-Julian oscillation. *PNAS*, **41 (24)**, 9158–9165, https://doi.org/10.1002/2014GL062518.

Powell, S. W., and R. A. Houze Jr., 2015: Effect of dry large-scale vertical motions on initial mjo convective onset. *Journal of Geophysical Research: Atmospheres*, **120 (10)**, 4783–4805, https://doi.org/https://doi.org/10.1002/2014JD022961, URL https://agupubs.onlinelibrary.wiley.com/doi/abs/10.1002/2014JD022961, https://agupubs.onlinelibrary.wiley.com/doi/pdf/10.1002/2014JD022961.

Roundy, P. E., 2014: Some aspects of western hemisphere circulation and the madden–julian oscillation. *Journal of the Atmospheric Sciences*, **71 (6)**, 2027–2039, https://doi.org/10.1175/JAS-D-13-0210.1, URL https://doi.org/10.1175/JAS-D-13-0210.1, https://doi.org/10.1175/JAS-D-13-0210.1.

Roundy, P. E., 2017: Diagnosis of seasonally varying regression slope coefficients and application to the mjo. *Quarterly Journal of the Royal Meteorological Society*, **143 (705)**, 1946–1952, https://doi.org/10.1002/qj.3054, URL https://rmets.onlinelibrary.wiley.com/doi/abs/10.1002/qj.3054, https://rmets.onlinelibrary.wiley.com/doi/pdf/10.1002/qj.3054.

Roundy, P. E., 2020: Interpretation of the spectrum of eastward-moving tropical convective anomalies. *Quarterly Journal of the Royal Meteorological Society*, **146 (727)**, 795–806, https://doi.org/10.1002/qj.3709, URL https://rmets.onlinelibrary.wiley.com/doi/abs/10.1002/qj.3709, https://rmets.onlinelibrary.wiley.com/doi/pdf/10.1002/qj.3709.

Roundy, P. E., 2022: Effect of advection by upper-tropospheric background zonal wind on mjo phase speed. *Journal of the Atmospheric Sciences*, **79 (7)**, 1859 – 1864, https://doi.org/10.1175/JAS-D-21-0298.1, URL https://journals.ametsoc.org/view/journals/atsc/79/7/JAS-D-21-0298.1.xml.

Roundy, P. E., and C. J. Schreck III, 2009: A combined wave-number–frequency and time-extended eof approach for tracking the progress of modes of large-scale organized tropical convection. *Quarterly Journal of the Royal Meteorological Society*, **135 (638)**, 161–173, https://doi.org/https://doi.org/10.1002/qj.356, URL https://rmets.onlinelibrary.wiley.com/doi/abs/10.1002/qj.356, https://rmets.onlinelibrary.wiley.com/doi/pdf/10.1002/qj.356.

Rui, H., and B. Wang, 1990: Development characteristics and dynamic structure of tropical intraseasonal convection anomalies. *Journal of the Atmospheric Sciences*, **47 (3)**, 357–379, https://doi.org/10.1175/1520-0469(1990)047⟨0357:DCADSO⟩2.0.CO;2, URL https://doi.org/10.1175/1520-0469(1990)047⟨0357:DCADSO⟩2.0.CO;2, https://doi.org/10.1175/1520-0469(1990)047⟨0357:DCADSO⟩2.0.CO;2.

Sakaeda, N., and P. E. Roundy, 2015: The development of upper-tropospheric wind over the western hemisphere in association with mjo convective initiation. *Journal of the Atmospheric Sciences*, **72 (8)**, 3138–3160, https://doi.org/10.1175/JAS-D-14-0293.1, URL https://doi.org/10.1175/JAS-D-14-0293.1, https://doi.org/10.1175/JAS-D-14-0293.1.

Salby, M. L., and H. H. Hendon, 1994: Intraseasonal Behavior of Clouds, Temperature, and Motion in the Tropics. *Journal of the Atmospheric Sciences*, **51 (15)**, 2207–2224, https://doi.org/10.1175/1520-0469(1994)051⟨2207:IBOCTA⟩2.0.CO;2, URL https://

doi.org/10.1175/1520-0469(1994)051⟨2207:IBOCTA⟩2.0.CO;2, https://journals.ametsoc.org/jas/article-pdf/51/15/2207/3426987/1520-0469(1994)051_2207_ibocta_2_0_co_2.pdf.

Shaaban, A., and P. Roundy, 2021: Upward and downward atmospheric kelvin waves across different speeds over the indian ocean. *Quarterly Journal of the Royal Meteorological Society*, **nan (nan)**, nan – nan, https://doi.org/nan, URL nan.

Shaaban, A. A., and P. E. Roundy, 2017: Olr perspective on the indian ocean dipole with application to east african precipitation. *Quarterly Journal of the Royal Meteorological Society*, **143 (705)**, 1828–1843, https://doi.org/10.1002/qj.3045, URL https://rmets.onlinelibrary.wiley.com/doi/abs/10.1002/qj.3045, https://rmets.onlinelibrary.wiley.com/doi/pdf/10.1002/qj.3045.

Sobel, A., S. Wang, and D. Kim, 2014: Moist Static Energy Budget of the MJO during DYNAMO. *Journal of the Atmospheric Sciences*, **71 (11)**, 4276–4291, https://doi.org/10.1175/JAS-D-14-0052.1, URL https://doi.org/10.1175/JAS-D-14-0052.1, https://journals.ametsoc.org/jas/article-pdf/71/11/4276/3817318/jas-d-14-0052_1.pdf.

Sobel, A. H., J. Nilsson, and L. M. Polvani, 2001: The weak temperature gradient approximation and balanced tropical moisture waves. *Journal of the Atmospheric Sciences*, **58 (23)**, 3650 – 3665, https://doi.org/https://doi.org/10.1175/1520-0469(2001)058⟨3650:TWTGAA⟩2.0.CO;2, URL https://journals.ametsoc.org/view/journals/atsc/58/23/1520-0469_2001_058_3650_twtgaa_2.0.co_2.xml.

Sperber, K. R., 2003: Propagation and the Vertical Structure of the Madden–Julian Oscillation. *Monthly Weather Review*, **131 (12)**, 3018–3037, https://doi.org/10.1175/1520-0493(2003)131⟨3018:PATVSO⟩2.0.CO;2, URL https://doi.org/10.1175/1520-0493(2003)131⟨3018:PATVSO⟩2.0.CO;2, https://journals.ametsoc.org/mwr/article-pdf/131/12/3018/4205340/1520-0493(2003)131_3018_patvso_2_0_co_2.pdf.

Stachnik, J. P., D. E. Waliser, and A. J. Majda, 2015: Precursor Environmental Conditions Associated with the Termination of Madden–Julian Oscillation Events. *Journal of the Atmospheric Sciences*, **72 (5)**, 1908–1931, https://doi.org/10.1175/JAS-D-14-0254.1, URL https://doi.org/10.1175/JAS-D-14-0254.1, https://journals.ametsoc.org/jas/article-pdf/72/5/1908/3668447/jas-d-14-0254_1.pdf.

Straub, K. H., 2013: Mjo initiation in the real-time multivariate mjo index. *Journal of Climate*, **26 (4)**, 1130–1151, https://doi.org/10.1175/JCLI-D-12-00074.1, URL https://doi.org/10.1175/JCLI-D-12-00074.1, https://doi.org/10.1175/JCLI-D-12-00074.1.

Trenberth, K. E., J. T. Fasullo, and J. Mackaro, 2011: Atmospheric Moisture Transports from Ocean to Land and Global Energy Flows in Reanalyses. *Journal of Climate*, **24 (18)**, 4907–4924, https://doi.org/10.1175/2011JCLI4171.1, URL https://doi.org/10.1175/2011JCLI4171.1, https://journals.ametsoc.org/jcli/article-pdf/24/18/4907/3980667/2011jcli4171_1.pdf.

Wang, B., and H. Rui, 1990: Synoptic climatology of transient tropical intraseasonal convection anomalies: 1975?1985. *Meteorology and Atmospheric Physics*, **44 (1-4)**, 43–61, https://doi.org/10.1007/BF01026810.

Wang, L., T. Li, E. Maloney, and B. Wang, 2017: Fundamental Causes of Propagating and Nonpropagating MJOs in MJOTF/GASS Models. *Journal of Climate*, **30 (10)**, 3743–3769, https://doi.org/10.1175/JCLI-D-16-0765.1, URL https://doi.org/10.1175/JCLI-D-16-0765.1, https://journals.ametsoc.org/jcli/article-pdf/30/10/3743/4676607/jcli-d-16-0765_1.pdf.

Wang, L., T. Li, and T. Nasuno, 2018: Impact of rossby and kelvin wave components on mjo eastward propagation. *Journal of Climate*, **31 (17)**, 6913 – 6931, https://doi.org/10.1175/JCLI-D-17-0749.1, URL https://journals.ametsoc.org/view/journals/clim/31/17/jcli-d-17-0749.1.xml.

Wheeler, M. C., and H. H. Hendon, 2004: An All-Season Real-Time Multivariate MJO Index: Development of an Index for Monitoring and Prediction. *Monthly Weather Review*, **132 (8)**, 1917–1932, https://doi.org/10.1175/1520-0493(2004)132⟨1917:AARMMI⟩2.0.CO;2, URL https://doi.org/10.1175/1520-0493(2004)132⟨1917:AARMMI⟩2.0.CO;2, https://journals.ametsoc.org/mwr/article-pdf/132/8/1917/4213489/1520-0493(2004)132_1917_aarmmi_2_0_co_2.pdf.

Wilks, D., 2011: *Statistical Methods in the Atmospheric Sciences*. Academic Press, Elsevier Science, URL https://books.google.com/books?id=IJuCVtQ0ySIC.

Yule, G. U., 1907: On the theory of correlation for any number of variables, treated by a new system of notation. *Proceedings of the Royal Society of London. Series A, Containing Papers of* *a Mathematical and Physical Character*, **79 (529)**, 182–193, URL http://www.jstor.org/stable/92723.

Zhang, C., 2005: Madden-julian oscillation. *Reviews of Geophysics*, **43 (2)**, https://doi.org/10.1029/2004RG000158, URL https://agupubs.onlinelibrary.wiley.com/doi/abs/10.1029/2004RG000158, https://agupubs.onlinelibrary.wiley.com/doi/pdf/10.1029/2004RG000158.

Zhang, C., and S. P. Anderson, 2003: Sensitivity of Intraseasonal Perturbations in SST to the Structure of the MJO. *Journal of the Atmospheric Sciences*, **60 (17)**, 2196–2207, https://doi.org/10.1175/1520-0469(2003)060⟨2196:SOIPIS⟩2.0.CO;2, URL https://doi.org/10.1175/1520-0469(2003)060⟨2196:SOIPIS⟩2.0.CO;2, https://journals.ametsoc.org/jas/article-pdf/60/17/2196/3467302/1520-0469(2003)060_2196_soipis_2_0_co_2.pdf.

Zhang, C., and M. Dong, 2004: Seasonality in the Madden–Julian Oscillation. *Journal of Climate*, **17 (16)**, 3169–3180, https://doi.org/10.1175/1520-0442(2004)017⟨3169:SITMO⟩2.0.CO;2, URL https://doi.org/10.1175/1520-0442(2004)017⟨3169:SITMO⟩2.0.CO;2, https://journals.ametsoc.org/jcli/article-pdf/17/16/3169/3786322/1520-0442(2004)017_3169_sitmo_2_0_co_2.pdf.

Zhao, C., T. Li, and T. Zhou, 2013: Precursor signals and processes associated with mjo initiation over the tropical indian ocean. *Journal of Climate*, **26 (1)**, 291–307, https://doi.org/10.1175/JCLI-D-12-00113.1, URL https://doi.org/10.1175/JCLI-D-12-00113.1.

Zhu, H., and H. H. Hendon, 2015: Role of large-scale moisture advection for simulation of the mjo with increased entrainment. *Quarterly Journal of the Royal Meteorological Society*, **141 (691)**, 2127–2136, https://doi.org/10.1002/qj.2510, URL https://rmets.onlinelibrary.wiley.com/doi/abs/10.1002/qj.2510, https://rmets.onlinelibrary.wiley.com/doi/pdf/10.1002/qj.2510.